THE ASTROPHYSICAL JOURNAL, 443:653–663, 1995 April 20

ULTRAVIOLET EXTINCTION TO 10.8 INVERSE MICRONS

PER A. AANNESTAD
Box 871504, Department of Physics and Astronomy, Arizona State University, Tempe, AZ 85287-1504
Received 1994 May 23; accepted 1994 October 27

ABSTRACT

UV extinction curves that represent observed variations in diffuse clouds (ζ Oph, ξ Per, and σ Sco) have been derived by combining *IUE* and *Voyager* data and have been modeled by a multicomponent size distribution of silicate and carbonaceous giants. We have used theoretical model atmospheres as our reddening-free standards, and, in the case of ζ Oph, also compare with the use of a stellar standard. An attempt was made to classify the UV spectra via theoretical spectral indices, but still missing line opacity appears to limit the use of this method at the present. The modeling includes five possible grain ingredients, large (0.015–0.25 μm) and small (0.005 μm) silicate grains, similarly large and small carbonaceous grains, and PAHs. The observed extinction curves are fitted by the model via nonlinear χ^2-minimization, varying the fractional amount of cosmic Si and C that are locked up in each ingredient. The observed variation from "steep" to "flat" UV extinction curves is found to correspond to a modest model variation in the lower limit of the power-law size distribution of the large grains. Graphite is found to be a necessary grain ingredient that cannot be replaced by the laboratory amorphous carbon materials. Carbonaceous mantles on the larger silicate grains provide no good fits to the observed curves. Using absorption properties of neutral laboratory PAHs limits PAHs to a few percent of the cosmic C abundance for acceptable fits that also give values for R_V close to the observed values.

Subject headings: dust, extinction — ultraviolet: ISM

1. INTRODUCTION

It has been well established for a long time that the interstellar ultraviolet extinction shows large variations from one line of sight to another (for a review, see Mathis 1990). Systematic differences exist among the diffuse clouds, and changes in relatively few parameters apparently describe the variations fairly well (Fitzpatrick & Massa 1986, 1988; Cardelli, Clayton, & Mathis 1989). A broad range of UV behavior is represented by the ζ Oph and σ Sco extinction curves, spanning the range from a very steep far-UV curve to a very flat curve in the far-UV, respectively (Snow 1992). Although other stars may show even more extreme behavior (cf. Cardelli & Savage 1988), it is the object of this paper to focus on the general range of variation as exhibited by ζ Oph and σ Sco. Some of the UV extinction variability appears due to environmental differences between dark clouds and regions of bright nebulosity, and the formation of mantles on small particles has been suggested as a possible physical process (Cardelli & Clayton 1991). We shall here model the extinction curves by considering variations in the size distribution, as well as in the shape and composition, including mantle formation, of the dust grains.

In investigating the far-UV extinction variations, it is important to consider as short wavelengths as possible. Any small grain population will manifest itself the strongest at the shortest wavelengths. Also, parameterizations obtained at longer wavelengths can be checked, to provide a test for additional grain characteristics that must be included. In general, not many stars have observed extinction beyond 8 μm^{-1}, and few have curves that go to 10 μm^{-1}. Snow, Allen, & Polidan (1990) presented extinction curves for eight stars from $\sim$6–10.8 μm^{-1} based on *Voyager* data and found that all showed a general rise in the far-UV. As part of an investigation into the UV and IR characteristics of dust in H II regions, we have derived extinction curves for some of the same stars over the range 3.2–10.8 μm^{-1} by combining archival data from the *IUE* and the *Voyager* data banks. Our "pair" method differs from that of Snow et al. since we use computed model atmospheres (Kurucz 1992) as nonreddened standards. The uncertainty due to dereddening of the comparison star, especially at far-UV wavelengths, is thus removed. We also attempt to classify the observed stars on the basis of their UV spectra, using the spectral index classification system of Fanelli, O'Connell, & Thuan (1987). Finally, we model the resulting extinction curves by considering mixtures of silicate and carbonaceous grains with varying size distributions, including the presence of mantles on the larger silicate grains.

2. OBSERVATIONAL DATA

We have selected the stars ζ Oph, ξ Per, and σ Sco as stars that span much of the variation in UV extinction for moderately reddened stars [$E(B-V) \approx 0.3$–0.4). In addition, we use the star μ Col as a standard in the usual "pair comparison" method for ζ Oph, in order to have a check on the present method of using model atmosphere standards. For each star, we have used two sets of short- and long-wavelength *IUE* spectra, and these are listed in Table 1, together with the source of the *Voyager* data. The *IUE* and *Voyager* data have been joined at a wavelength of 1178 Å. *IUE* data obtained before 1988 were reprocessed by the National Space Science Data Center as of 1993 July, and all images were reduced locally by the use of RDAF software. The low-resolution spectra have been corrected for time degradation. Only data points flagged as "good" (EPS value of 100) have been used. The SW and LW images have been joined (not interpolated) at wavelengths in the range of 1900–1950 Å, and we see no significant zero-point shifts between the two cameras in the present data. All observations are large aperture observations. In the case of ξ Per and σ Sco, no low-resolution spectra were present in the *IUE* data bank, and we instead used available high-resolution images, and averaged these by weights into bins of width 3 Å.

TABLE 1

UV DATA

Star	HD Number	*IUE* Images	*Voyager* Number	Date	Spectrum Number	Shift (Å)
ξ Per	24912	SWP 37373 LWR 14987	1	1981 Mar 22	1[a]	0
		SWP 37376 LWR 14988	2	1980 Jun 26	2[a]	0
σ Sco	147165	SWP 11064 LWP 18630	1	1980 Jun 25	1[a]	0
		SWP 39508 LWP 18631	1	1980 Jun 25	2[a]	0
ζ Oph	149757	SWP 32894 LPW 12637	2	1984 Dec 12	1	+2.0
		SWP 18252 LWR 14381	2	1984 Dec 12	2	+1.0
μ Col[b]	38666	SWP 25386 LWR 17657	1	1981 Oct 8	1	+1.5
		SWP 41195 LWP 19996	1	1981 Oct 8	2[a]	0

[a] *IUE* high-resolution data of bin widths 3 Å.
[b] Comparison star for ζ Oph.

As a check on the binning procedure, we have included a set of high-resolution images for μ Col. No time degradation corrections exist for high-resolution data. However, the low-resolution degradation corrections (up to 1988) are of the order of 10% or less, which is about the same as the uncertainty in the absolute calibration of the *IUE*. At this level, none of the conclusions here are significantly affected.

Finally, due to the poor wavelength calibration of the low-resolution spectra at wavelengths below 1300 Å, we have shifted these spectra by an amount necessary to move the center of the Lyα absorption feature to 1215.7 Å. This shift is listed in the last column of Table 1.

The observed spectra have to be corrected for atomic and molecular hydrogen absorption along the line of sight. In correcting for H I Lyα absorption we have followed the procedure of Fitzpatrick & Massa (1990) by convolving the absorption profile due to H I with the instrumental Gaussian, using values for the interstellar hydrogen column density as given by Diplas & Savage (1994). However, because of the low S/N and possible geocoronal emission in the central part of the profile, we have deleted the region 1190–1240 Å from the spectra. In addition, in order to remove spurious structure in the extinction due to small wavelength differences between the observed and the model spectra, we have deleted data at the Lβ and Lγ wavelengths of 1025 and 970 Å, respectively.

For the molecular hydrogen correction, we have made use of synthetic H_2 spectra smeared to the resolution of the *Voyager* spectrometers (Snow, Allen, & Polidan 1990; Polidan 1993). For an H_2 column density as given by Bohlin, Savage, & Drake (1978) the H_2 relative absorption was linearly interpolated and divided into the observed spectrum.

3. MODEL STANDARDS

The usual "pair" method relies on finding an unreddened or slightly reddened comparison star of the same spectral class as the observed star. However, it is often difficult to find an exact spectral match, and a mismatch of even one spectral subclass can lead to large errors in the ultraviolet extinction. Also, any dereddening of the comparison standard according to some "average" extinction curve provides an additional source of error. As shown by Boggs & Böhm-Vitense (1989), instead using theoretical energy distributions for comparison may lead to smaller errors, as long as the model continuum matches the continuum of real stars to a good approximation. The model energy distributions of Kurucz (1979) for hotter stars ($T_{\rm eff} >$ 30,000 K) work well in this respect, as long as the wavelength $\lambda > 1700$ Å (Boggs & Böhm-Vitense 1989; Böhm-Vitense, Hodge, & Boggs 1984). At the shorter wavelengths, these models do not have enough opacity, leading to an overestimate of the extinction. However, in the recent models of Kurucz (1992) a large number of additional line opacities as well as additional continuum opacities have been included, and extensive model grids in $T_{\rm eff}$ and log g are provided at a resolution of 10 Å. While there still may be deficiencies in the ultraviolet opacities, and there are uncertainties in the model input parameters such as $T_{\rm eff}$, log g, abundances, and microturbulent velocities, using the intrinsically reddening-free model standards should give no more uncertain far-UV extinction than the traditional method. As a check on the relative agreement between the two procedures, we also derive the extinction curve for ζ Oph by comparing with its usual standard μ Col.

A fundamental difficulty in deriving an ultraviolet extinction curve is classifying the UV spectrum correctly in order to find the correct unreddened UV standard. A reddened star with the same MK spectral class as an unreddened comparison star may not have the same intrinsic energy distribution in the ultraviolet part of the spectrum. Fanelli et al. (1987) have defined a set of 12 far-UV spectral line indices based on *IUE* low-resolution spectra that may serve as temperature, luminosity, and abundance discriminants, since line indices are quite unaffected by the unknown continuum extinction. The most direct way of picking a comparison model on this basis would be to compare the observed line indices with calculated theoretical indices as functions, of $T_{\rm eff}$, log g, abundance, and other input parameters. However, limitations in the current Kurucz models for hot stars such as the lack of non-LTE, no inclusion of wind effects, and some opacity still missing, make calculated line indices quite uncertain. Comparing the observed indices with the empirical list of indices versus spectral class given by Fanelli et al. (1992) and then converting to temperature and gravity via the usual calibrations, is a less direct, but maybe "safer" way of obtaining a good comparison. Nevertheless, since not all theoretical line indices are equally subject to the mentioned limitations, we have used the models to calculate four selected indices as additional guides in choosing the model standard. Also, such calculations provide an estimate of how close the present Kurucz LTE models approximate some of the far-UV line absorptions.

One of the lines selected is the Si IV λ1397 line, since it is a diagnostic for late-O to early B stars, peaking at around spectral type B1 (Fanelli et al. 1992). Being a strong resonance line, it could be influenced by the presence of a wind, but for main-sequence stars the wind effect is actually not present (Walborn & Panek 1984). The line could be affected by non-LTE effects,

although primarily in its core. In addition to the Si IV line we have selected three blended lines, BL 1425 (Fe V, C III, and Si III), Fe V λ1453, and BL 1617 (Fe IV and Fe V) (Fanelli et al. 1992). The effects of non-LTE are lessened in blended lines of the same element and ionization stage because of many additional radiative pathways being present. Also, since these are blends of many weaker lines, they should not be much affected by the presence of a stellar wind.

The wavelength resolution of the Kurucz (1992) models as published is 10 Å while the line indices are defined as integrals over bandpasses typically only 20 Å in width. It is therefore necessary to recompute the theoretical spectra at a much higher resolution. Courtesy R. Kurucz (1993, personal communication), we have computed synthetic spectra at a resolution $\Delta\lambda/\lambda = 50{,}000$ for the wavelength intervals of the four indices mentioned above. We have assumed solar abundances for the models, and the microturbulent velocity has been set to 2 km s^{-1}. The spectra have been rotationally broadened with a rotational velocity of 25 km s^{-1}, and smeared with a Gaussian profile corresponding to the *IUE* low-resolution instrumental profile of FWHM = 6.1 Å. The UV line index is defined as $-2.5 \log_{10} F_\lambda/F^c_\lambda$, where F_λ is the average flux density for the band in question and F^c_λ is the linearly interpolated flux density at the center of the band computed from the average flux densities in two bracketing sidebands (Fanelli et al. 1992).

In Figure 1 we show the four theoretical indices as functions of $T_{\rm eff}$ and log g, as well as the observed line indices for seven main-sequence stars (point stars) and five giant stars (luminosity class III) (point circles) as tabulated by Fanelli et al. (1992). In plotting the latter, we have assumed the spectral class versus $T_{\rm eff}$ calibration given by Schmidt-Kaler (1982). The stars are of a spectral class B2 or earlier and should therefore have metal abundances similar to solar, as assumed in the model spectra calculated here. The error bars represent an estimate of the minimum uncertainty in the spectral index using a relative uncertainty in the *IUE* flux levels of 0.03 (Massa, Savage, & Fitzpatrick 1983). The limiting upper temperature for the models, given a value of log g, is set by the model becoming unstable due to radiative acceleration ("blow-up"). We see that the model calculations show the same trend with temperature as the observed indices and are within the observational uncertainties for the lower temperatures. However, at the higher temperatures there appears to be a systematic overestimate of the line flux relative to the continuum by ~10% (change of 0.1 in the index). This is most probably due to still missing model line opacity, but this should not seriously affect the derived extinction, which is more sensitive to model continuum opacity. In the case of the BL 1425 index, there appears to be a constant offset of ~0.05 over the whole temperature range, which could be applied as an "empirical" correction to the present models. However, given the observational uncertainty in this relatively weak feature and its weak temperature dependence, any derived temperature will have a large uncertainty. Considering all the far-UV indices in Figure 1, it does not appear possible at the present time to use these indices to determine an effective temperature to better than a few thousand degrees. On the other hand, this is comparable to the uncertainty of about one MK spectral subclass estimated for the "pair" method.

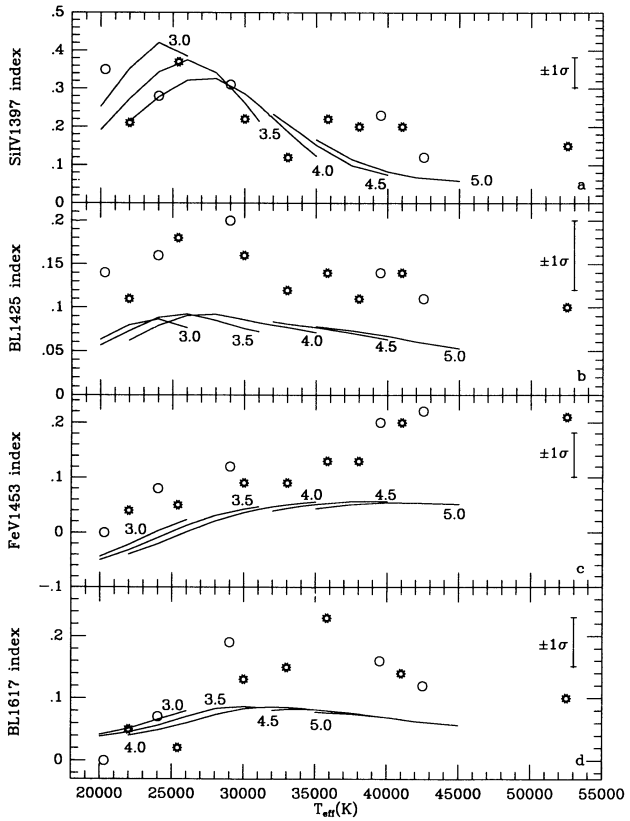

FIG. 1.—*Lines:* theoretical line indices as functions of the effective stellar temperature computed from the models of Kurucz (1992). Values of log g as indicated. *Circles and stars:* observed line indices for main-sequence stars and giants respectively (from Fanelli et al. 1992).

TABLE 2

FAR-UV STELLAR INDICES AND MODEL STANDARDS

Star	Type	Spectrum	Si IV λ1397	BL 1425	Fe V λ1453	BL 1617	$T_{\rm eff}$, log g[a]
ξ Per.....	O7.5	1	0.17	0.12	0.16	0.26	35,000 4.0
		2	0.14	0.13	0.16	0.25	...
σ Sco	B1 III	1	0.34	0.10	0.05	0.11	25,000 3.5
		2	0.39	0.12	0.02	0.13	...
ζ Oph.....	O9.0 V	1	0.18	0.16	0.11	0.17	35,000 4.0
		2	0.19	0.13	0.09	0.20	...
μ Col	O9.5 V	1	0.19	0.11	0.04	0.19	33,000 4.0
		2	0.21	0.15	0.08	0.19	...

[a] Selected Kurucz grid model standard.

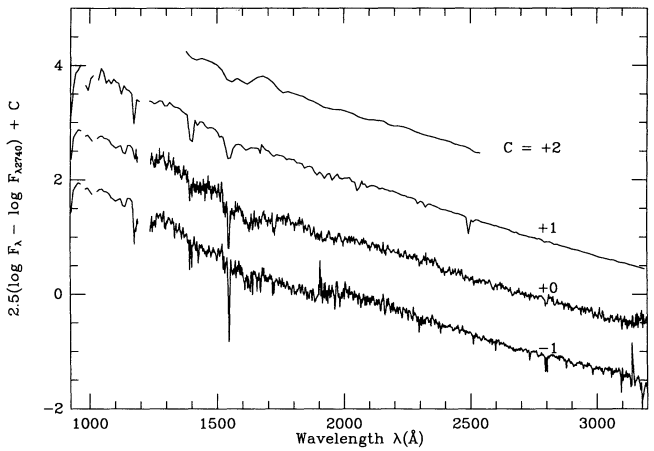

FIG. 2.—Spectra normalized to the flux at 2740 Å with arbitrary offsets of C. Curve for C = 0, the dereddened [$E(B-V) = 0.01$] spectrum of μ Col using low-resolution *IUE* data and *Voyager* data. Curve for C = −1, the μ Col spectrum using binned high-resolution *IUE* data. Curve for $C = +1$, the spectrum from the Kurucz (1992) model with $T_{\rm eff} = 33{,}000$ K log $g = 4.0$, and solar abundances. Curve for C = +2, the empirical intrinsic flux distribution for O9.5 V stars (Papaj et al. 1990).

In Table 2 we list the far-UV line indices as determined from the *IUE* spectra of Table 1. The Kurucz grid model standard selected on the basis of these values and the Fanelli et al. observed values in Figure 1 are listed in the last column of Table 2. For the O stars, the model value of log g is the grid value closest to the value for the particular star as determined from fundamental parameters as estimated by Howarth & Prinja (1989). For the B stars, the value is chosen based on the calibration tables of Schmidt-Kaler (1982).

In Figure 2 we compare the Kurucz model of $T_{\rm eff} = 33{,}000$ K, log $g = 4.0$ with the two observed spectra of μ Col as well as with the intrinsic flux distribution for O9.5 V stars as deduced from two-color diagrams by Papaj, Wegner, & Krelowski (1990). The spectra are normalized to the flux density at 2740 Å and shifted relative to each other by one dex for visibility. The μ Col spectra have been dereddened by applying an average UV extinction curve (Seaton 1979) for $E(B-V) = 0.01$. The binned high-resolution spectrum shows a small intensity shift at 1900 Å due to photometric differences between the *IUE* short and long-wavelength cameras, but otherwise is in good agreement with the low-resolution spectrum. However, we caution that no extensive study of using degraded high-dispersion data for extinction calculations has been done, and that we have only demonstrated the utility of this for the present data set. Finally, we see that the Kurucz model continuum agrees very well both with the observed spectra of μ Col and with the O9.5 V intrinsic spectrum, even for wavelengths below 1700 Å. It appears that current modelling can reasonably account for the far-UV continuum, justifying our use of the models as reddening-free standards.

4. UV EXTINCTION CURVES

The normalized extinction curves $E(\lambda) = E(\lambda - V)/E(B-V)$ derived here are calculated according to

$$E(\lambda) = \frac{-2.5 \log \{[F(\lambda)/F(V)][F_0(\lambda)/F_0(V)]\}}{B-V-(B-V)_0} . \quad (1)$$

$F(\lambda)$ and $F_0(\lambda)$ are the intensities of the observed star and the model spectrum, respectively. $F_0(V)$ is the model mean intensity as averaged over the visual $S(\lambda)_0$ filter function given by Matthews & Sandage (1963). $F(V)$ is the mean intensity outside Earth's atmosphere as calculated from (using the same filter function) log $F(V) = -0.4\ V - 8.45$, where V is the observed visual magnitude. $B-V$ is the observed color index and the model $(B-V)_0$ is calculated from the filter functions as proscribed by Matthews & Sandage. Before forming the ratios in equation (1), the *IUE* data were averaged in bins of equal width of 0.05 μm^{-1}. The input values used in deriving the extinction for each star is listed in Table 3, and the extinction curves for each spectrum of ζ Oph, ξ Per, and σ Sco are shown in Figure 3. The "gaps" are due to spurious structure removed near the hydrogen lines, the C IV line, and, for ζ Oph and ξ Per, near the Si IV line. For ζ Oph, we also show the extinction curves (dashed curves in Fig. 3*a*) derived from the "pair" comparison method using the dereddened and hydrogen-corrected spectrum 1 of μ Col (Table 1) as the standard spectrum. In this case we took $E(B-V) = B-V-(B-V)_0 = 0.32$ (Diplas & Savage 1993). Except for a slightly flatter minimum beyond the 4.6 μm^{-1} extinction hump, using a computed model standard gives good agreement with the traditional "pair" method for the whole range of wavelengths.

In modeling these extinction curves, we shall assume a multicomponent size distribution of dust grains. There is a set of "very small grains" (Rayleigh limit) of dimension 50 Å, and a distribution $n(a) \propto a^{-3.5}$ of larger, spherical grains with radii in the range $a_{\rm min}$ to $a_{\rm max}$, where the smallest value of $a_{\rm min}$ is 0.0156 μm, and the largest value of $a_{\rm max}$ is 0.25 μm. As shown by Draine & Malhotra (1993), it is necessary for an accurate calculation of wavelength-dependent extinction that the distribution of radii is such that $a_{i+1}/a_i \leq 1.15$. We therefore subdivide the range $a_{\rm min}$ to $a_{\rm max}$ into 20 size bins. These larger grains are made of separate populations of silicate and carbonaceous (graphite or amorphous) grains, and the silicate grains may have a mantle of constant thickness, made of either graphitic material, amorphous carbon, or "organic refractory" material. The optical constants of silicate and graphite are taken from Draine (1985) and Draine & Lee (1984), respectively. For amorphous carbon we choose the optical properties as either

TABLE 3

INPUT DATA AND $E(B-V)$

Star	log N(H)[a]	log $N(H_2)$[b]	V[a]	$B-V$[a]	$E(B-V)$[a]	$E(B-V)$[c]
ξ Per.....	21.05	20.52	4.03	0.01	0.33	0.32
σ Sco	21.38	19.79	2.88	0.13	0.39	0.40
ζ Oph.....	20.69	20.64	2.56	0.02	0.32	0.33
μ Col	19.84	15.5	5.16	−0.29	0.01	...

[a] Diplas & Savage 1993.
[b] Bohlin et al. 1978.
[c] Present model calculation

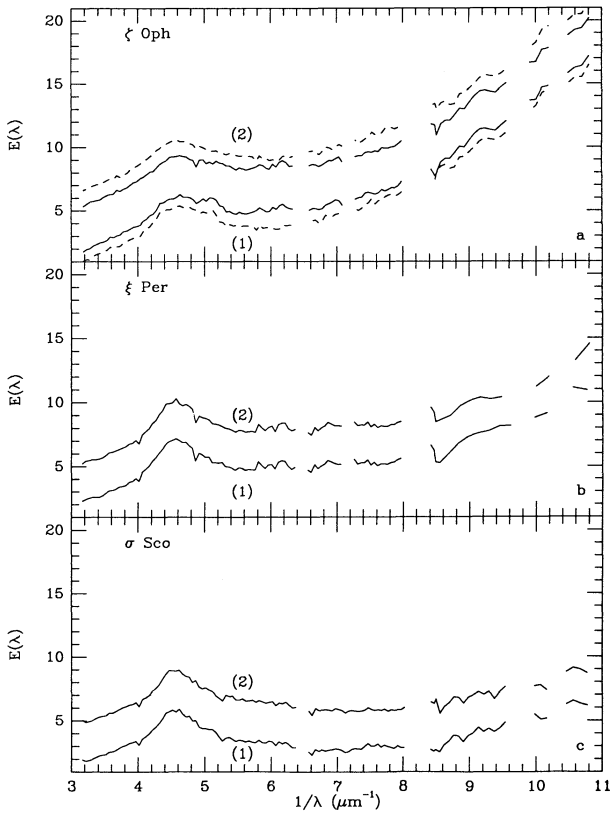

FIG. 3.—Normalized extinction curves derived from the spectra (1 and 2) of Table 1. *Solid curves:* using Kurucz model standards as listed in Table 2. Curves (2) have been arbitrarily displaced upward by 3 units for clarity. *Dashed curves:* μ Col as standard (ζ Oph only). For clarity, dashed curves (1) and (2) have been displaced by -1 and $+4$ units, respectively.

given by Hageman, Gudat, & Kunz (1974), by the AC1 or BE1 optical constants of Rouleau & Martin (1991), or by Edoh's (1983) constants as listed by Hanner (1987).[1] The optical constants of the organic refractory material are from Table 3 of Jenniskens (1993). The very small grains are assumed to have the composition of either graphite, the amorphous carbon types given above, or diamond. The optical properties of diamond are from Papadopoulos & Anastassakis (1991). Extinction cross sections are calculated via Mie-type calculations for homogenous spheres and coated spheres (Bohren & Huffman 1983). For the small graphite particles we also calculated extinction due to disks or anisotropic ellipsoids, using the Discrete Dipole Approximation (Draine 1988). In addition, we include a component of polycyclic aromatic hydrocarbons (PAHs), with absorption cross sections from Figure 1 of Joblin, Léger, & Martin (1992) and from Puget & Léger (1989).

A given model thus has five possible ingredients, large and small silicate grains, large and small carbonaceous grains, and the PAHs. In addition, the large silicate grains may have mantles. After choosing the detailed material compositions, and the ranges for the size distributions of the larger grains, we fit the model extinction to the observed extinction curve by nonlinear χ^2-minimization, varying the fractional amount of cosmic Si and C that are locked up in each ingredient. Calculations covering a range of compositions, and different size ranges indicate through the χ^2- value what constitutes the "best" fit. If the ratio of visual to selective extinction (R_V) is known, we also require that the model gives a value close to observed value. It is important to note that since we are fitting to *relative* extinction values, only the relative fractional amounts of Si and C get determined. Changing all the fractional depletions in the various ingredients by one and the same factor produces the identical $E(\lambda)$ and R_V. The values given in the figures are values that are closest to the absolute level of visual extinction. Also, the assumed cosmic abundances of C and Si (C/H $= 4.7 \times 10^{-4}$ [Lambert 1978], Si/H $= 3.5 \times 10^{-5}$) determine the relative and absolute levels of extinction. The solar carbon abundance may be lower by $\sim 15\%$ (C/H $= 4 \times 10^{-4}$; Grevesse et al. 1991), and the model fractional dust amounts should then be increased by a factor of 1.18. Finally, the material densities assumed are 3.3 g cm^{-3} for silicate, 2.3 g cm^{-3} for graphite, 1.5 g cm^{-3} for amorphous carbon, and 3.5 g cm^{-3} for diamond.

While we have searched in the somewhat arbitrarily limited parameter space of $[a_{\rm min}, a_{\rm max}] = [0.0156\ \mu{\rm m}, 0.25\ \mu{\rm m}]$ for the best-fit solutions, there is no absolute guarantee that a set of very different values cannot give equally good or better fits. An extensive global optimization program over a much larger region and including simultaneously all the possible material ingredients would be valuable, but is outside the scope of this investigation. In some cases we have included seven simultaneous ingredients (small and large silicates, small and large graphite, small and large amorphous carbon, and PAHs), but without significantly changed results.

For the random errors in the observational data we assume (Massa, Savage, & Fitzpatrick 1983)

$$\sigma[E(\lambda)] = \frac{\{\sigma_1^2 + 2.25 \times 10^{-4}[1 + E^2(\lambda)]\}^{1/2}}{E(B-V)} . \qquad (2)$$

For *IUE* observations $\sigma_1 \approx 0.03$, while for the *Voyager* data $\sigma_1 \approx 0.05$. For the *Voyager* part of the stellar spectrum we have the additional uncertainty due to the H_2 correction, and we estimate that in this range the total error is $\sigma_1 \approx 0.07$.

The systematic errors due to incorrect $T_{\rm eff}$ or log g can be investigated by calculating extinction curves based on different Kurucz model standards. However, for the hottest chosen standard (log $g = 4.0$, $T_{\rm eff} = 37{,}500$ K), no stable models exist for a higher temperature. We have therefore calculated relative extinction curves at the nearest model grid point where models for $T_{\rm eff} \pm 2000$ K and log $g \pm 0.5$ do exist, assuming that approximately the same ratios apply at the higher temperatures. For each program star we calculate an "upper" and a "lower" extinction curve corresponding to variations in $T_{\rm eff}$ of ± 2000 K and in log g of ± 0.25.

In Figure 4*a* we show the extinction curve for ζ Oph obtained from co-adding the two spectra (solid curves) in Figure 3*a*, using the Kurucz model (Table 2) as the standard. The bars denote the random errors at each wavelength point as calculated from equation (2). The dashed line is the "best-fit" model, and the solid curves represent the systematic "error envelope" (no random error included) as discussed above. Indicated in the figure are the cosmic fractions of Si and C present in each grain population. Substituting any of the amorphous carbon grains for the graphite grains in this figure

[1] Note that the entry in Table 2-1 of Hanner (1987) of the value for n for $\lambda = 0.90\ \mu$m should read 2.02.

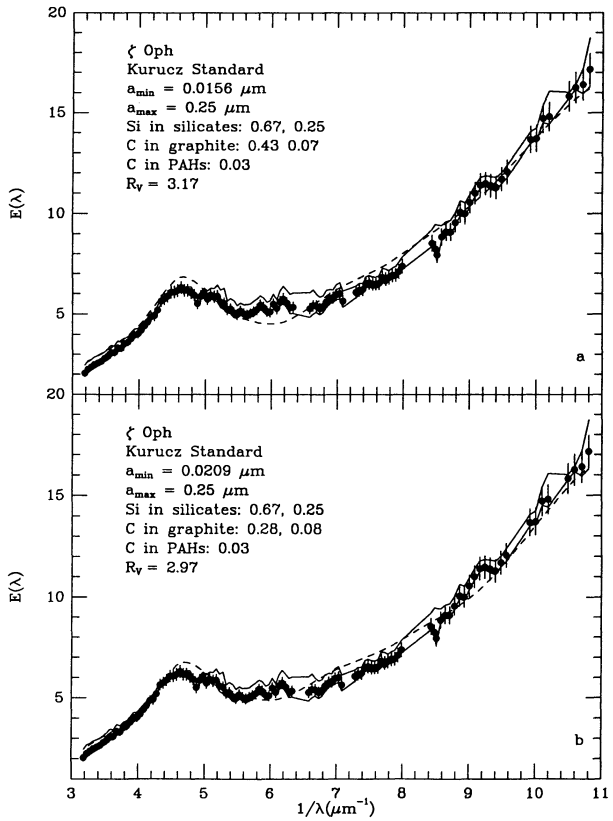

FIG. 4.—*Dashed curves:* χ^2-fits to co-added, normalized extinction data (see Fig. 3*a*) for ζ Oph with a theoretical model standard. Bars show 1 σ observational errors. *Solid curves:* observed extinction curves for a comparison model variation of ± 2000 K in $T_{\rm eff}$ and ± 0.25 in log g. Dust model parameters as indicated. Si and C values refer to the fraction of cosmic abundances tied up in the larger grains and in the very small grains, respectively. R_V is the model value for the ratio of visual to selective extinction.

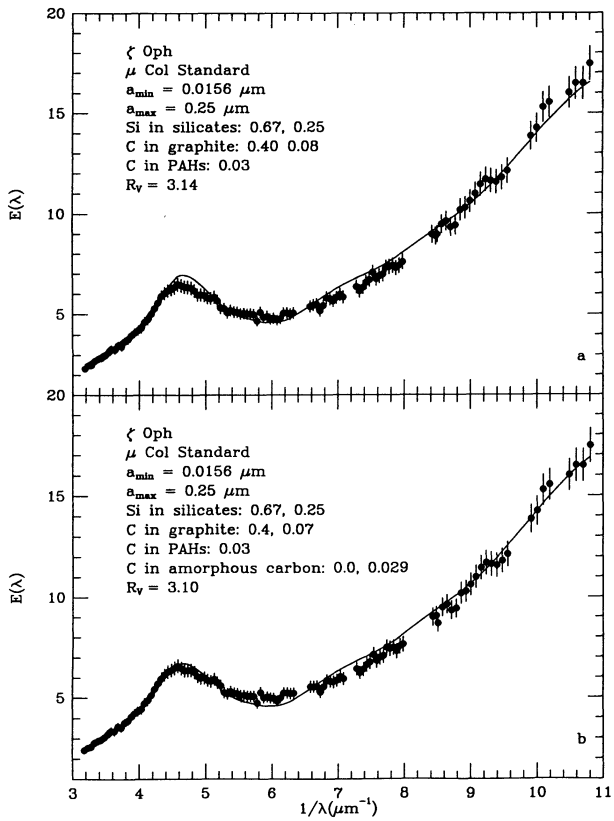

FIG. 5.—*Solid curves:* χ^2-fits to co-added, normalized extinction data for ζ Oph with μ Col as standard star. Notation as in Fig. 4. Note the better fit at ~ 6 μm^{-1} compared to Fig. 4.

or adding a mantle of amorphous carbon to the silicates cannot give reasonable agreement with the observed curve, although a simultaneous presence of large and small amorphous carbon grains at the level of a few percent in the carbon fraction cannot be ruled out. An increase in the carbon PAH fraction from 0.03 to 0.075 with a simultaneous decrease in the graphite fractions (to 0.33 and 0.05) would give a slightly better fit, but the R_V value would be significantly too low (2.7) compared to the observed value of 3.09 (Cardelli et al. 1989). The main discrepancies between the model extinction and the observations in Figure 4*a* is a predicted slightly higher extinction peak at 4.6 μm^{-1} and a lower minimum at ~ 6 μm^{-1}. The latter can be slightly improved by changing $a_{\rm min}$ from 0.0156 μm to 0.021 μm, as shown in Figure 4*b*, although the extinction peak then moves to ~ 4.7 μm^{-1} and the predicted R_V value decreases to 2.93. However, if we instead fit the ζ Oph extinction curve using μ Col as the standard, the fits in this region are significantly improved, as shown in Figure 5. Figure 5*a* shows the co-added extinction (dashed curves in Fig. 3*a*) with the same model curve as in Figure 4*a*. The χ^2-value decreases by more than a factor of 2. This may indicate that the Kurucz model standards used for ζ Oph are slightly deficient in continuum opacity in the particular wavelength interval of 1600–1800 Å as compared to real stars. Adding a small amount of amorphous carbon (BE1) as very small grains further improves the fit, but only slightly, as shown in Figure 5*b*.

In Figure 6 we show the best-fit models for ξ Per, for which the observed R_V value is 3.40 (Cardelli et al. 1989). These fits differ from the ζ Oph case mainly in the lack of very small (0.005 μm) silicate grains and in no PAHs being present above a level of a few percent of the cosmic abundance of carbon. The graphite peak in Figure 6*a* is at slightly shorter wavelengths than in the observations, and an overall better fit is achieved by changing the 0.005 μm spherical graphite grains to oblate ellipsoids of axial ratio 2:1 and the same volume ($a_{\rm VSG,equiv} = 0.005$ μm), and increasing the minimum size for the larger graphite grains from 0.016 to 0.04 μm. This is shown in Figure 6*b*. As in the case of ζ Oph, but to a smaller degree, we note the increased extinction relative to the model in the region around 6 μm^{-1}, possibly indicating a slight deficiency in Kurucz model opacity for this region.

Figure 7 shows the results for σ Sco. The strong deviation in the lower envelope curve from the data points is mostly due to the sensitivity of the far-UV flux to a decrease in temperature of the model atmosphere from 25,000 to 23,000 K. As shown in Figure 7*a*, the flat UV extinction can be very well fit by imposing a lack of both silicate and graphite grains with sizes in the range 0.01–0.04 μm, and no presence of PAHs above a few percent of the cosmic carbon abundance. However, the graphite peak is clearly at too short wavelengths, and Figure 7*b* shows a much improved fit by again, as in the case of ξ Per, replacing the spherical very small graphite grains with 2:1 oblate ellipsoids. In both cases the predicted R_V values are close to the observed value of $R_V = 3.80$ (Cardelli et al. 1989).

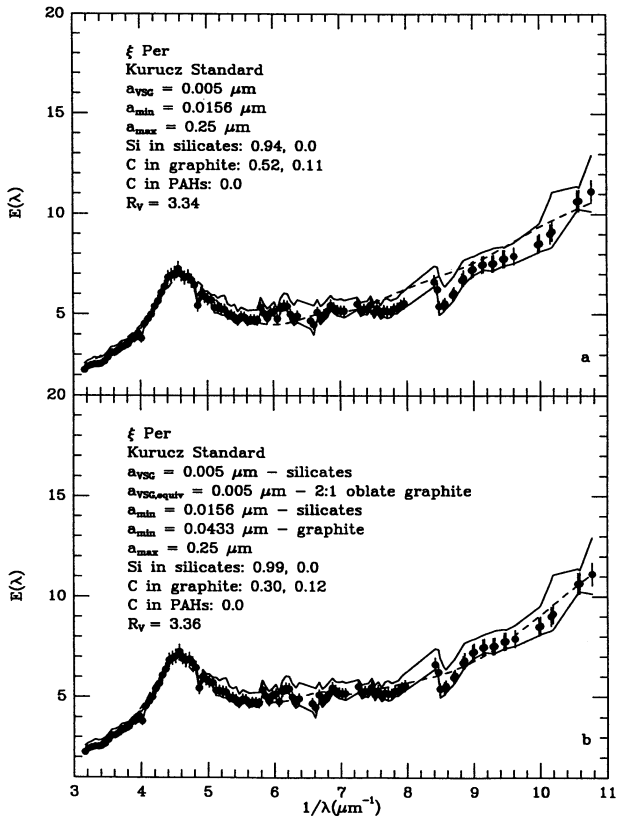

FIG. 6.—*Dashed curves:* χ^2-fits to co-added, normalized extinction data (Fig. 3*b*) for ξ Per. Notation as in Fig. 4.

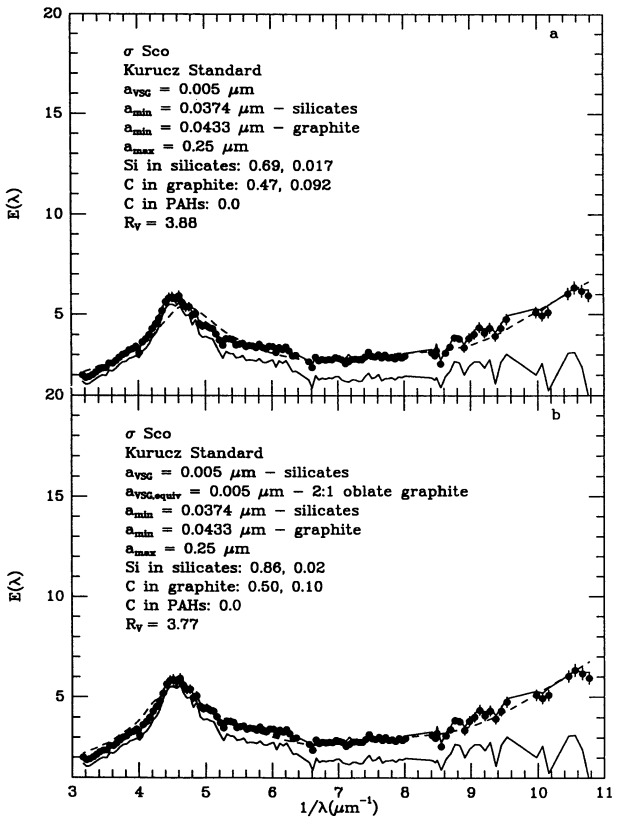

FIG. 7.—*Dashed curves:* χ^2-fits to co-added, normalized extinction data (Fig. 3*c*) for σ Sco. Notation as in Fig. 4.

5. DISCUSSION

The UV extinction curves derived here for ζ Oph, ξ Per, and σ Sco using theoretical comparison models agree well with those derived by others using the stellar pair comparison method (Bless & Savage 1972; York et al. 1973; Clayton & Hanson 1993). Having theoretical models as reddening-free standards is of great value in determining interstellar extinction curves. From the present work, the recent models of Kurucz (1992) appear to be quite good in providing the continuum from which one derives extinction, even at far-UV wavelengths, although more comparisons with the "pair method" are desirable. One limitation of the present model atmospheres is "blow-up" due to radiative acceleration, which limits modeling to stars later than about O8 for $\log g \leq 4.0$. Even more important, modeling cannot yet provide a consistent calibration of the UV spectrum through selected line indices, as was attempted here. Additional line opacities, non-LTE effects, and stellar winds may all have to be included before a spectral match to better than a few thousand degrees can be achieved. On the other hand, the quantitative differences found between the theoretical and observed line indices (Fig. 1), although systematic, are of the order of the uncertainty in the observed values. Given the complexity of line formation in hot stellar atmospheres, the differences are perhaps surprisingly small.

We have assumed a model grain population of silicate and carbon grains plus molecular-sized PAHs, with a possible carbonaceous mantle of constant thickness on the larger silicate grains. Although not unique, these ingredients are the ones most often considered responsible for extinction in diffuse interstellar clouds (Mathis 1990). Interstellar graphitic material has been positively identified in the Murchison carbonaceous meteorite via its isotopic composition (Bernatowicz et al. 1991). The Duley/Williams model (Williams 1989) in which the 4.6 μm^{-1} feature is due to $(OH)^-$ ions in very small silicate grains has not been considered, nor have we considered "fluffy" grains (Mathis & Whiffen 1989) or fractal grains (Wright 1989). A power-law size distribution as assumed here is expected on theoretical grounds from the shattering of larger particles into smaller particles (Bierman & Harwit 1979). In addition, we have assumed sets of "very small" grains in the Rayleigh limit that may be the "end result" of destructive processes for the larger grains. Since in this limit the extinction/unit volume is independent of grain size, a size distribution need not be specified, and we have assumed a single size of 0.005 μm. This size is perhaps the smallest size for which bulk optical constants can still be used with some confidence (Huffman 1988). Near-infrared continuum emission may determine the actual size of such particles through the strong dependence of temperature fluctuations on the grain size.

Our main result is that the observed variation in the ultraviolet extinction curves can be accounted for through independent variations in the relative numbers of large and small graphite and silicate grains, an important factor being only modest variations in the lower limit of the size distribution (a_{min} = 0.01–0.04 μm). Green et al. (1992) also found that larger grains than "normal" were required to explain the "anomalous" UV extinction curve of ρ Oph (similar to the curve for σ Sco), although they could not get a good fit at the shortest wavelengths ($1/\lambda \geq 10$ μm^{-1}). A good fit may,

however, be achieved if independent variations in a very small grain population is allowed, as we have done in this work. Using our model with $a_{min} = 0.028$ and 0.0433 μm for silicates and graphite, respectively, and 2:1 oblate, very small graphite grains we find depletion values of 0.49 and 0.10 for the silicate grains (large and small) and 0.58 and 0.11 for the graphite grains. The value of R_V is 4.31, close to the observed value of 4.34 (Cardelli et al. 1989). The model hump position is at slightly too long wavelengths (4.50 μm^{-1} instead of 4.59 μm^{-1}), but less oblate grains can easily fit the observed position (spherical grains would move the position to 4.65 μm^{-1}). Thus similar size deviations from the "normal" size distribution as deduced earlier, but with somewhat different relative numbers of silicate and graphite grains can also account for the extinction difference between ρ Oph and σ Sco.

A similar dust distribution with just silicate and graphite grains was found to be consistent with several correlations in observed UV extinction curves (Aannestad 1992), although as shown by Draine & Malhotra (1993), the claim that random variations in the relative depletion factors of Si and C would lead to the observed lack of correlation between the central wavelength of the 4.6 μm^{-1} feature and its width was not correct. There is at present no explanation for this lack of a detailed correlation. Draine & Malhotra (1993) conclude that variations in the dielectric properties of the small grains due to either surface effects, degree of crystallinity, or impurities may be responsible, but this remains to be experimentally verified. However, we note that according to Jenniskens & Greenberg (1993), H II regions may follow the predicted decrease of hump width with decreasing central wavelength.

Destructive processes (e.g., in high-velocity shocks) may turn larger grains into smaller as well as into gaseous form, and intrinsic variations in the orginal ratios of small and large particles should also be expected. However, if the present model of the variations is correct, it is necessary to find a plausible mechanism through which $\sim$0.01 μm size grains are preferentially destroyed or removed relative to both larger *and* smaller grains in the cases where the UV extinction curve is found to be "flat." It is possible that simultaneous sticking and shattering processes under dense enough conditions will have such an effect on a size distribution. Another possible process is radiation pressure which, depending on the spectrum of the radiation, will selectively accelerate some particles more than others. We have calculated the ratio of the radiation pressure force to the gravitational force as a function of grain size for the stellar spectra considered here. Normalizing to the ratio for the very small silicate grains, the results show that for a relatively cooler star of 25,000 K (B1 III in σ Sco), the ratio peaks at a radius of $\sim$0.02 μm, being $\sim$1–1.6 for silicates and $\sim$2–3 for graphite, for the relevant radii in the range 0.01–0.04 μm. Only some of the reason for the systematically larger ratio of graphite grains is due to their lower specific weight (2.25 g cm^{-3}) compared the silicate grains (3.3 g cm^{-3}). A 35,000 K spectrum gives no similar, preferentially high ratio for intermediate size-grains, consistent with the "nonflat" extinction curve of ζ Oph. On the other hand, other forces would also influence the dynamics of the dust, such as gas drag and, in particular, plasma drag if the dust is in an ionized region. We note that σ Sco has a O9.5 V secondary star that may contribute ionizing photons. (Clayton & Hanson 1993 showed that including flux from this star would have no significant affect on the extinction curve). Only a detailed dynamical treatment can decide if stellar radiation pressure is a viable mechanism for changing the dust size distributions as implied from these fits to the extinction curves.

In our calculations we find that very similar UV extinction curves can be obtained with quite different silicate-graphite mixtures and values for a_{min}. The value of R_V provides an important constraint, and is also a particular sensitive measure of the upper size limit, as long as $a_{max} \leq 0.25$ μm. However, the abrupt cutoff at 0.25 μm is clearly nonphysical, and a smooth and exponential decrease beginning at $\sim$0.2 μm, such as deduced by Kim, Martin, & Hendry (1994) would be more appropriate. These authors, using a maximum entropy method to deduce the details of silicate-graphite size distributions in the case of extinction curves with $R_V = 3.1$ and 5.3, found relative deficiencies in small- and intermediate-size grains for the "flat" extinction curve ($R_V = 5.3$) in qualitative agreement with the results here.

The mean variation in diffuse cloud extinction curves has been empirically parameterized by the value of R_V (Cardelli et al. 1989). However, important deviations from this simple average relationship take place with decreasing wavelengths and increasing values of R_V. Mathis & Cardelli (1992) have investigated the deviations for various types of line-of-sight environments. The deviations for the present stars are shown in Figure 8, where the extinction data for ζ Oph, ξ Per, and σ Sco are plotted together with fits according to the prescription of Fitzpatrick & Massa (1988) and with R_V-parameterized curves. Although it may be possible to find a better single-parameter fit to the diffuse extinction curves, such a fit can

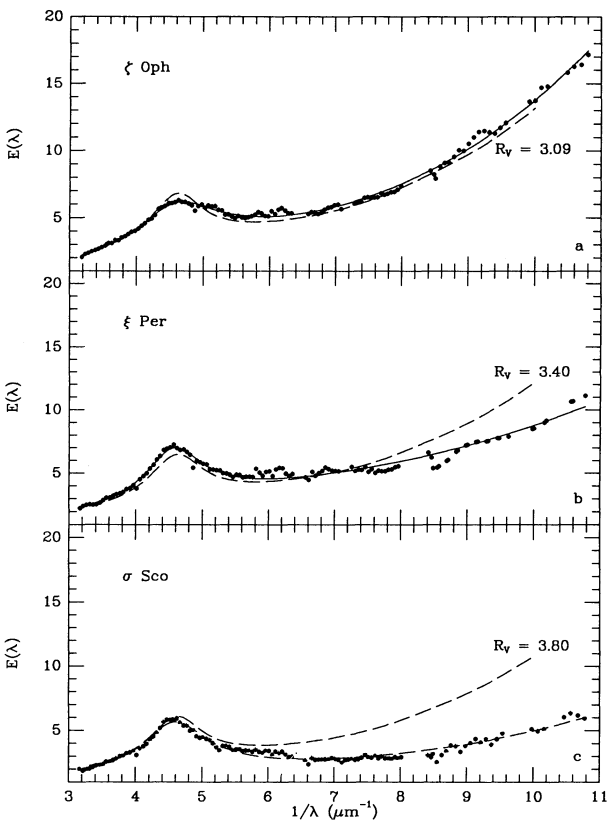

FIG. 8.—*Filled circles:* observed extinction values for ζ Oph, ξ Per, and σ Sco. *Solid curves:* fits according to the prescription of Fitzpatrick & Massa (1988). *Dashed curves:* R_V parameterized curves according to Cardelli et al. (1989).

obviously only be a rough guide to the effects of the varying numbers of small- and intermediate-size grains explored here.

Environmental differences between lines of sight often provide clues to the nature of the extinction curve, with the reddening per unit distance as a rough discriminator (Fitzpatrick & Massa 1988). However, the widely different curves of ζ Oph and σ Sco correspond to about the same value (2.3 and 2.7 mag kpc^{-1}, respectively), while the intermediate case of ξ Per has a much lower value (0.9 mag kpc^{-1}). Clearly, other factors must be important, such as whether the associated star is embedded in the cloud or not, and the nature of the radiation field (Snow 1992). Jenniskens & Greenberg (1993) distinguish between the diffuse medium (DIF), warm gas surrounding OB associations (BUB), and compact H II regions (HII). In terms of the parameter scheme of Fitzpatrick & Massa (1988), they find a systematically lower value for the linear rise (c_2) in the case of BUB and HII compared to DIF, while HII have a systematically low value for the hump parameter (c_3) compared to the other two environments. From the fits as shown in Figure 8, this would place the environment of ζ Oph ($c_2 = 0.89$, $c_3 = 6.8$) in the DIF category, and σ Sco ($c_2 = 0.2$, $c_3 = 5.2$) in the H II category. Although ξ Per has a low value for the hump parameter ($c_3 = 4.5$), it has a large value for the linear rise ($c_1 = 0.7$), and thus does not fall neatly into any of these classes. Also, the data of Jennisken & Greenberg (1993) show no variation in the far-UV nonlinear rise between the three environments, while the value for σ Sco deduced here ($c_4 = 0.14$) is a factor of 3 smaller than for ζ Oph ($c_4 = 0.45$).

It is often suggested that the extinction variation as seen in σ Sco–type cases is due to coatings on grains that are not coated under ζ Oph–type conditions. Grain mantles composed of H_2O, CO, and hydrocarbons are present under molecular cloud conditions and may also be present in some diffuse clouds toward the Galactic center (McFadzean et al. 1989). In the calculations here, we have attempted to fit the σ Sco extinction curve with either amorphous carbon or "organic refractory" material as the mantle material on the silicate grains, as well as replacing graphite grains with the various amorphous carbon grains. In general, no satisfactory fits could be found with these materials included, unless they accounted for less than a few percent of the cosmic carbon abundance and graphite particles also were allowed at about their "normal" abundance. A size distribution very different from the power law assumed here may give a different result, but the 4.6 μm^{-1} hump will in no case be fitted well by the amorphous carbon materials. We note that amorphous carbon exposed to UV radiation or to cosmic rays in diffuse clouds is likely to be converted into a graphitic material (Duley 1993).

Since small diamond grains ($\sim$10 Å) have been found in carbonaceous meteorites (for a review see Anders & Zinner 1993) and their predicted interstellar abundance via shock processing may correspond to 10%–20% of the carbon abundance (Tielens et al. 1987), they may form an important constituent of interstellar dust. Diamond grains cannot substitute for graphite grains since no 4.6 μm^{-1} feature is present for small diamond particles. However, such particles may account for a large fraction of the far-UV rise if they are included along with graphite particles. Their extinction efficiency for $1/\lambda \geq 6$ μm^{-1} is similar to that of the small silicate particles, and they may therefore be substituted for such grains without changing the extinction curve substantially. For example, an equally good fit as that in Figure 4*a* is obtained by decreasing the fraction of Si in small silicate grains from 0.25 to only 0.07, while adding to the mixture small diamond grains (50 Å) with a carbon fraction of 0.26. For Figure 4*b*, correspondingly, the small silicates would account for 0.14 of the Si and the diamond particles for 0.16 of the C. Using the optical properties of the meteoritic microdiamonds (Lewis, Anders, & Draine 1989), there is less of a change, with good fits given by the fractions 0.18, 0.033, and 0.22, 0.019 for Figures 4*a* and 4*b*, respectively. The sharp absorption edge of diamond at 5.6 μm^{-1} is not readily detected in these cases, even for a fractional carbon abundance in diamonds as large as 0.2–0.3.

Another model that includes amorphous carbon invokes graphitization of the carbon to form the 4.6 μm^{-1} feature and various degrees of hydrogenation to explain the strong variability in the far-UV (Hecht 1986; Sorrell 1990). Recent experimental results (Colangeli et al. 1993) show some support for this, but again the hump feature is very broad and appears at too long wavelengths (4.2 μm^{-1}). Lack of knowledge of the optical constants of hydrogeneated amorphous materials prevents detailed testing of this model.

The UIR features in the near-infrared are usually ascribed to emission by PAH-like molecules or particles, emitting energy absorbed at UV wavelengths, and they should therefore contribute to the UV extinction. We found that including the present PAHs (Joblin et al. 1992) at a level of more than a few percent of the cosmic carbon abundance made the UV extinction fits worse. Although these PAHs have a strongly increasing far-UV absorption cross section, the hump feature is too broad and at two short wavelengths ($\sim$5.8 μm^{-1}) to fit the interstellar feature. Some PAHs also have a strong secondary feature at $\sim$3.6–3.8 μm^{-1} (Joblin 1994) that is not present in the interstellar extinction curves. In addition, the value of R_V is sensitive to the presence of these PAHs. For example, in the case of ξ Per (Fig. 5*b*) R_V decreased from 3.36 to 3.05 when PAHs were added and accounting for a carbon abundance of only 5%. However, our present knowledge of the optical properties of PAH materials is limited, and we note that Schutte, Tielens, & Allamandolla (1993) use a relatively constant cross section in the UV/visible for a size distribution of small PAHs. Also, PAHs are expected to be ionized under interstellar conditions, and ionized species may have very different absorptive properties from the neutral material properties assumed here (Lee & Wdowiak 1993). Salama & Allamandola (1992) obtained a UV/visible absorption cross section for $C_{10}H_8^+$ about two orders of magnitude larger per C atom than for ordinary PAHs. Although PAHs (or other materials) are clearly *not required* to fit the UV extinction variations in diffuse clouds, as ionized species they may still be important contributors to the extinction curve.

One constraint that has not been taken into account here, is the absolute value of the extinction. Using the column density of hydrogen (H + H_2) along a line of sight, the model predicts a visual extinction which can be compared with the product of the observed color excess $E(B-V)$ and the value of R_V. For example, for ζ Oph the observed visual extinction is $\sim$1 mag, while the curves in Figures 4 and 5 correspond to only 0.6 mag. Increasing the dust abundance significantly would violate the cosmic constraint on Si, and selectively increasing the absorption in the visible might change the shape of the extinction curve. It may be that this problem reflects uncertainties in the cosmic abundances in this direction, which have been assumed solar. For ξ Per and σ Sco, however, the model depletions (Figs. 6 and 7) give visual extinctions in agreement with the observed to within 0.1 mag.

If depletion values for Si and C could be accurately determined in the various lines of sight, these model calculations could be directly checked. The depletion of C relative to the depletion of Si should be considerably higher in the σ Sco case compared to that of ζ Oph. However, such determinations are difficult, reflecting both difficulties in observing weak interstellar lines and uncertainties in atomic parameters. The GHRS instrument on the *Hubble Space Telescope* provide new capabilities, and Sofia et al. (1994) have recently determined element depletions from earlier data in the directions of ζ Oph (Cardelli et al. 1993), ξ Per (Cardelli et al. 1991), and other stars. Assuming solar abundances as reference abundances (C/H $= 4 \times 10^{-4}$, Si/H $= 3.5 \times 10^{-5}$), they find that 0.95 of the Si and 0.63 (range of 0.54–0.72) of the C is in the dust phase for the main absorbing component toward ζ Oph. Corrected to their reference abundance for C, our Figures 4 and 5 have the values 0.92 and 0.6 for Si and C, respectively, except for Figure 4*b* which has 0.36 for C. For ξ Per they give a value of 0.37 for C with error limits at 0.19 and 0.54. The corresponding value in Figure 6*b* is 0.49. Cardelli et al. (1993) suggest a conversion of solid carbon (graphite) into gaseous carbon as a (partial) reason for the relatively lower amount of carbon in the dust phase in the case of ξ Per. No measurements of Si were made in the direction of ξ Per. It would be important to obtain accurate elemental depletions in many directions characterized by both steep and flat far-UV extinction curves.

An unexpected result from the Sofia et al. (1994) observations in the direction of ζ Oph is that 0.61 of the O solar abundance should be present in the dust, corresponding to 15 O atoms for every Si atom. In ordinary silicates such as assumed here (e.g., olivines, pyroxines) the O/Si ratio is only 3–4. Perhaps the silicates are hydrated silicates such as seen toward SN 1987A by Timmermann & Larson (1993), or many of the grains are oxides. In that case, calculations such as done here should be repeated with the relevant optical constants. However, if Sofia et al. (1994) use B star reference abundances, they obtain an O/Si ratio of 4, as expected for silicates. On the other hand, they find that the B star reference abundance for C is not likely to be valid, while the solar C reference abundance is quite acceptable. It may be that relative element abundances vary substantially from place to place, which would greatly complicate our understanding of the detailed composition of the dust and the testing of extinction models.

Finally, the interstellar grain albedo a and the scattering asymmetry parameter g may also put constraints on the dust models pursued here. Recent analysis of the interstellar far-ultraviolet radiation field (Henry & Murthy 1993) show that large values ($a > 0.5$, $g > 0.7$) at far-UV wavelengths are consistent both with diffuse ultraviolet background measurements and with images of the reflection nebula NGC 7023, if an extragalactic background flux is assumed. Without a background flux, the values are considerably lower ($a \sim 0.3$, $g \sim 0.15$), and the grains in the reflection nebula must be assumed to be different from the dust at high galactic latitudes. For the grain mixture in Figures 4–6, the mean albedo at $\sim$1500 Å ranges from 0.35 to 0.45 and the asymmetry parameter varies from 0.6 to 0.75, with the larger values applying where the mean grain size is increased. While not quite as large as the values for the nebula NGC 2023, these values fall well within the preferred contours in the analysis of Henry & Murthy (1993).

6. CONCLUSIONS

The main conclusions to be drawn from our modeling of ultraviolet diffuse extinction curves by size distributions of silicate and carbonaceous grain mixtures are

1. Acceptable fits require that graphite is the main carbon component. The various amorphous carbon materials cannot substitute for the graphite grains, although such materials may present at the level of a few percent of the cosmic carbon abundance. Also, amorphous carbon or "organic refractory" mantles on the silicate grains do not provide acceptable fits to the present extinction curves. On the other hand, small diamond grains (Rayleigh limit) may substitute for some or most of the small silicate grains.
2. Using optical properties of laboratory PAHs gives model fits that limit the carbon fraction in neutral PAHs to a few percent at most. Also, a substantial presence of PAHs would tend to lower R_V to unacceptable levels. However, ionized species of PAHs may have quite different optical properties, and, although not required in the present fits, may still be important contributors to the UV extinction curve.
3. The range in the ultraviolet extinction curves as represented by the curves of ζ Oph and σ Sco can be understood as mostly due to a variation in the presence of grain sizes $\sim$0.01–0.04 μm. The "flat" extinction curve of σ Sco demands a lower limit for the power-law size distribution of $a_{\min} \sim 0.04$ μm, but with still a substantial number of grains in the Rayleigh limit (here 0.005 μm). The intermediate extinction curve of ξ Per can be similarly well modeled if no silicate Rayleigh-size particles are present.
4. The best fits to the 4.6 μm^{-1} extinction hump in the curves of ξ Per and σ Sco is obtained if the Rayleigh-size graphite grains are 2:1 oblate disks.
5. For $R_V \geq 3.4$, the far-UV extinction may deviate significantly from the mean R_V-dependent extinction law of Cardelli et al. (1989).
6. Theoretical stellar atmosphere models (Kurucz 1992) may be used as reddening-free comparisons, even at far-UV wavelengths, although some continuum opacity may still be missing in the region $\sim$1700 Å. Theoretical UV line indicates are systematically low compared to the observations and cannot at the present time be used for accurate spectral classification.

I am indebted to R. Kurucz for the use of his model atmospheres and spectral synthesis programs, to R. Polidan for the H_2 correction files, and to B. Draine for the use of the DDSCAT extinction program. I also want to thank P. Martin for sending data on amorphous carbon materials and C. Joblin for data on laboratory PAHs. Finally, I acknowledge useful discussions with D. Burstein and P. Hauschildt. This research was supported by NASA grant NAG 5-1743.

REFERENCES

Aannestad, P. A. 1992, ApJ, 386, 627
Anders, E., & Grevesse, N. 1989, Geochim. Cosmochim. Acta, 53, 197
Anders, E., & Zimmer, E. 1993, Meteoritics, 28, 490
Bernatowicz, T. J., Amari, S., Zinner, E. K., & Lewis, R. S. 1991, ApJ, 373, L73
Bierman, P., & Harwit, M. 1979, ApJ, 241, L33
Bless, R. C., & Savage, B. D. 1972, ApJ, 171, 293
Boggs, D., & Böhm-Vitense, E. 1989, ApJ, 339, 209
Bohlin, R. C., Savage, B. D., & Drake, J. F. 1978, ApJ, 224, 132
Böhm-Vitense, E., Hodge, P., & Boggs, D. 1984, ApJ, 287, 825
Bohren, C. F., & Huffman, D. R. 1983, Absorption and Scattering of Light by Small Particles (New York: Wiley)
Cardelli, J. A., & Clayton, G. C. 1991, AJ, 101, 1021
Cardelli, J. A., Clayton, G. C., & Mathis, J. S. 1989, ApJ, 345, 245
Cardelli, J. A., Mathis, J. S., Ebbets, D. C., & Savage, B. D. 1993, ApJ, 402, L17
Cardelli, J. A., & Savage, B. D. 1988, ApJ, 325, 864
Cardelli, J. A., Savage, B. D., Bruhweiler, F. C., Smith, A. M., Ebbets, D. C., Sembach, K. R., & Sofia, U. J. 1991, ApJ, 377, L57
Clayton, G. C., & Hanson, M. M. 1993, AJ, 105, 1880
Colangeli, L., Mennella, V., Blanco, A., Fonti, S., Bussoletti, E. Gumlich, H. E., Mertins, H. C., & Jung, C. H. 1993, ApJ, 418, 435
Diplas, A., & Savage, B. D. 1994, ApJ, 427, 274
Draine, B. T. 1985, ApJS, 57, 587
———. 1988, ApJ, 333, 848
Draine, B. T., & Lee, H. M. 1984, ApJ, 285, 89
Draine, B. T., & Malhotra, S. 1993, ApJ, 414, 632
Duley, W. W. 1993, in Dust and Chemistry in Astronomy, ed. T. J. Millar & D. A. Williams (London: IOP)
Edoh, O. 1983, Ph.D. thesis, Univ. of Arizona
Fanelli, M. N., O'Connell, R. W., Burstein, D., & Wu, C.-C. 1992, ApJS, 82, 197
Fanelli, M. N., O'Connell, R. W., & Thuan, T. X. 1987, ApJ, 321, 768
Fitzpatrick, E. L., & Massa, D. 1986, ApJ, 307, 286
———. 1988, ApJ, 328, 734
———. 1990, ApJS, 72, 163
Green, J. C., Snow, T. P., Cook, T. A., Webster, C. C., & Poplawski, O. 1992, ApJ, 395, 289
Grevesse, N., Lambert, D. L., Sauval, A. J., van Dishoeck, E. F., Farmer, C. B., & Norton, R. H. 1991, A&A, 242, 488
Hageman, H.-J., Gudat; W., & Kunz, C. 1974, Deutsches Electronen Synchrotron, SR-47/7 (Hamburg: Deutsches Electron-Synchrotron)
Hanner, M. S. 1987, in Infrared Observations of Comets Halley and Wilson and Properties of the Grains, NASA CP 3004, 22
Hecht, J. 1986, ApJ, 305, 817
Henry, R. C., & Murthy, J. 1993, ApJ, 418, L17
Howarth, I. D., & Prinja, R. K. 1989, ApJS, 69, 527
Huffman, D. R. 1988, in Optical Effects Associated With Small Particles, ed. P. W. Barber & R. K. Chang (Singapore: World Scientific), 279
Jenniskens, P. 1993, A&A, 274, 653
Jenniskens, P., & Greenberg, J. M. 1993, A&A, 274, 439
Joblin, C. 1994, private communication
Joblin, C., Léger, A., & Martin, P. 1992, ApJ, 393, L79
Kim, S.-H., Martin, P. G., & Hendry, P. D. 1994, ApJ, 422, 164
Kurucz, R. L. 1979, ApJS, 40, 1
——. 1992, in The Stellar Populations of Galaxies, ed. B. Barbuy & A. Renzini (Dordrecht: Kluwer), 225
Lambert, D. L. 1978, MNRAS, 182, 249
Lee, W. L., & Wdowiak, T. J. 1993, ApJ, 410, L127
Lewis, R. S., Anders, E., & Draine, B. T. 1989, Nature, 339, 117
Massa, D., Savage, B. D., & Fitzpatrick, E. L. 1983, ApJ, 266, 662
Mathis, J. S. 1990, ARA&A, 28, 37
Mathis, J. S., & Cardelli, J. A. 1992, ApJ, 398, 610
Mathis, J. S., & Whiffen, G. 1989, ApJ, 341, 808
Matthews, T. A., & Sandage, A. R. 1963, ApJ, 138, 30
McFadzean, A. D., Whittet, D. C. B., Longmore, A. J. L., Bode, M. F., Adamson, A. J. 1989, MNRAS, 241, 873
Papadopoulos, A. D., & Anastassakis, E. 1991, Phys. Rev., B, 43, 5090
Papaj, J., Wegner, W., & Krełowski, J. 1990, MNRAS, 246, 408
Polidan, R. S. 1993, private communication
Puget, J. L., & Léger, A. 1989, ARA&A, 27, 161
Rouleau, F., & Martin, P. G. 1991, ApJ, 377, 526
Salama, F., & Allamandola, L. J. 1992, ApJ, 395, 301
Schmidt-Kaler, Th. 1982, in Numerical Data and Functional Relationships in Science and Technology Group VI, Vol. 2b, ed. K. Schaifers & H. H. Voigt (Berlin: Springer), § 4, 453
Schutte, W. A., Tielens, A. G. G. M., & Allamandola, L. J. 1993, ApJ, 415, 397
Seaton, M. J. 1979, MNRAS, 187, 73P
Snow, T. P. 1992, Australian J. Phys., 45, 543
Snow, T. P., Allen, M. M., & Polidan, R. S. 1990, ApJ, 359, L23
Sofia, U. J., Cardelli, J. A., & Savage, B. D. 1994, ApJ, 430, 650
Sorell, W. H. 1990, MNRAS, 243, 570
Tielens, A. G. G. M., Seab, C. G., Hollenbach, D. J., & McKee, C. F. 1987, ApJ, 319, L109
Timmermann, R., & Larson, H. P. 1993, ApJ, 415, 820
Walborn, N. R., & Panek, R. J. 1984, ApJ, 280, L27
Williams, D. A. 1989, in Interstellar Dust, ed. L. J. Allamandola & A. G. G. M. Tielens (Dordrecht: Kluwer), 367
Wright, E. L. 1989, in Interstellar Dust, ed. L. J. Allamandola & A. G. G. M. Tielens (Dordrecht: Kluwer), 337
York, D. G., Drake, J. F., Jenkins, E. B., Morton, D. C., Rogerson, J. B., & Spitzer, L. 1973, ApJ, 182, L1